



Annunziata, F., Matyjaszkiewicz, A., Fiore, G., Grierson, C., Di Bernardo, M., Marucci, L., & Savery, N. (2017). An Orthogonal Multi-input Integration System to Control Gene Expression in *Escherichia coli*. *ACS Synthetic Biology*, 6(10), 1816-1824.
<https://doi.org/10.1021/acssynbio.7b00109>

Publisher's PDF, also known as Version of record

License (if available):
CC BY

Link to published version (if available):
[10.1021/acssynbio.7b00109](https://doi.org/10.1021/acssynbio.7b00109)

[Link to publication record in Explore Bristol Research](#)
PDF-document

This is the final published version of the article (version of record). It first appeared online via ACS at <http://pubs.acs.org/doi/abs/10.1021/acssynbio.7b00109>. Please refer to any applicable terms of use of the publisher.

University of Bristol - Explore Bristol Research

General rights

This document is made available in accordance with publisher policies. Please cite only the published version using the reference above. Full terms of use are available:
<http://www.bristol.ac.uk/red/research-policy/pure/user-guides/ebr-terms/>

An orthogonal multi-input integration system to control gene expression in *Escherichia coli*

Supplementary Information

FABIO ANNUNZIATA^{1,5}, ANTONI MATYJASZKIEWICZ^{2,5}, GIANFRANCO
FIORE^{2,5}, CLAIRE S. GRIERSON^{3,5}, LUCIA MARUCCI^{2,5}, MARIO DI
BERNARDO^{2,4,5}, NIGEL J. SAVERY^{1,5}

¹School of Biochemistry, University of Bristol, BS8 1TD, Bristol, UK

²Department of Engineering Mathematics, University of Bristol, BS8 1UB,
Bristol, UK

³School of Biological Sciences, University of Bristol, BS8 1UH, Bristol, UK

⁴Department of Electrical Engineering and Information Technology,
University of Naples Federico II, 80125, Naples, Italy

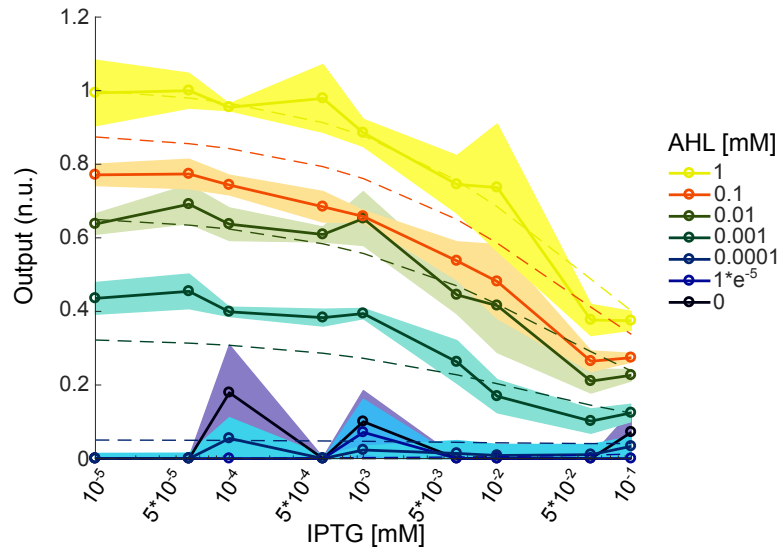
⁵BrisSynBio, Bristol, BS8 1TQ, UK

Contents

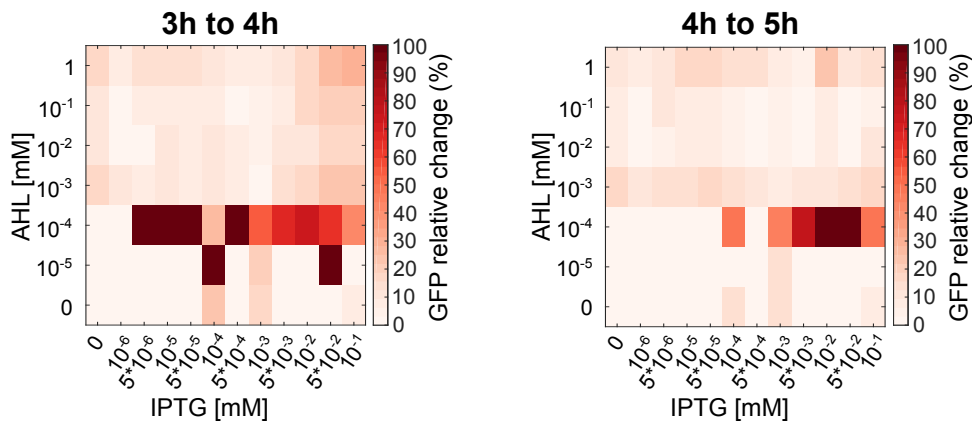
S1 Supplementary figures	1
S2 Model Derivation	11
S2.1 Model assumptions	11
S2.2 Summary of dynamical variables in the full model	12
S2.3 Reactions considered in the full model	13
S2.4 Dynamics of the full model	14
S3 Model simplification	18
S4 Parameter identification	20
S5 Cellular consortium and comparator model	22
References	24

S1 Supplementary figures

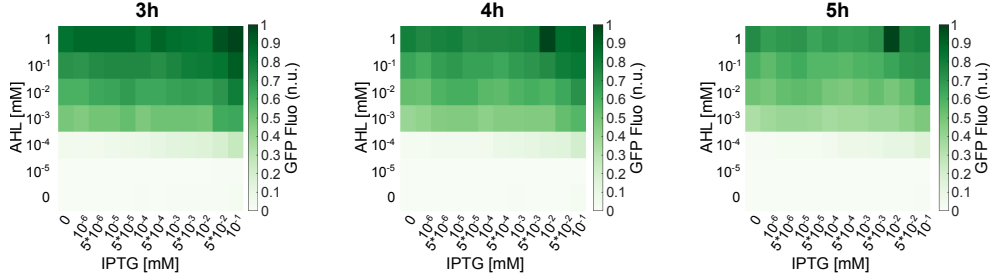
A)



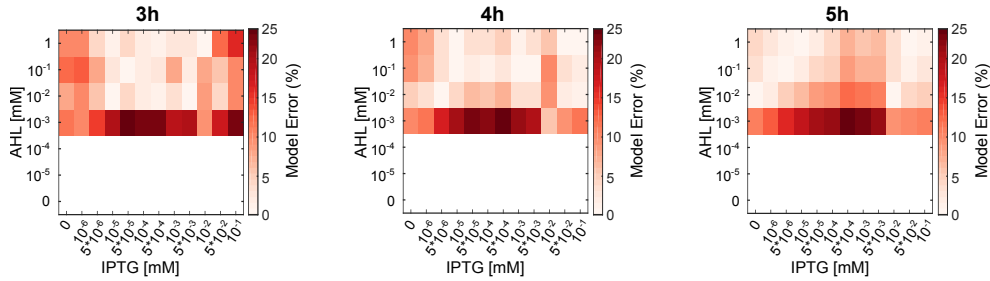
B)



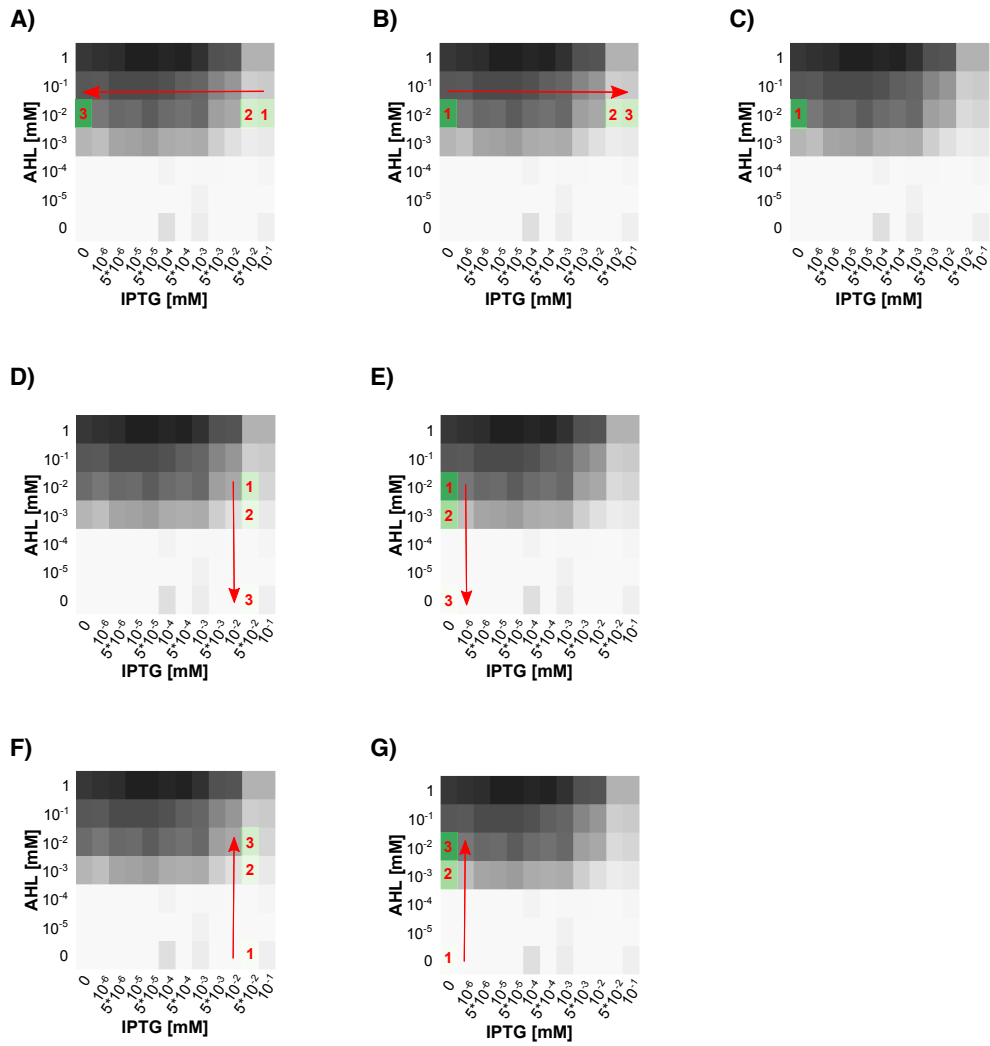
Supplementary Figure S1: Percentage change and responsive region in the GFP expression levels after signal computation. **A)** Observed responsive region for the wide range characterization (solid lines) and model simulations (dashed lines). \pm S.E.M. of three independent experiments is indicated by shaded area. **B)** Percentage of change between GFP values measured at the indicated time points.



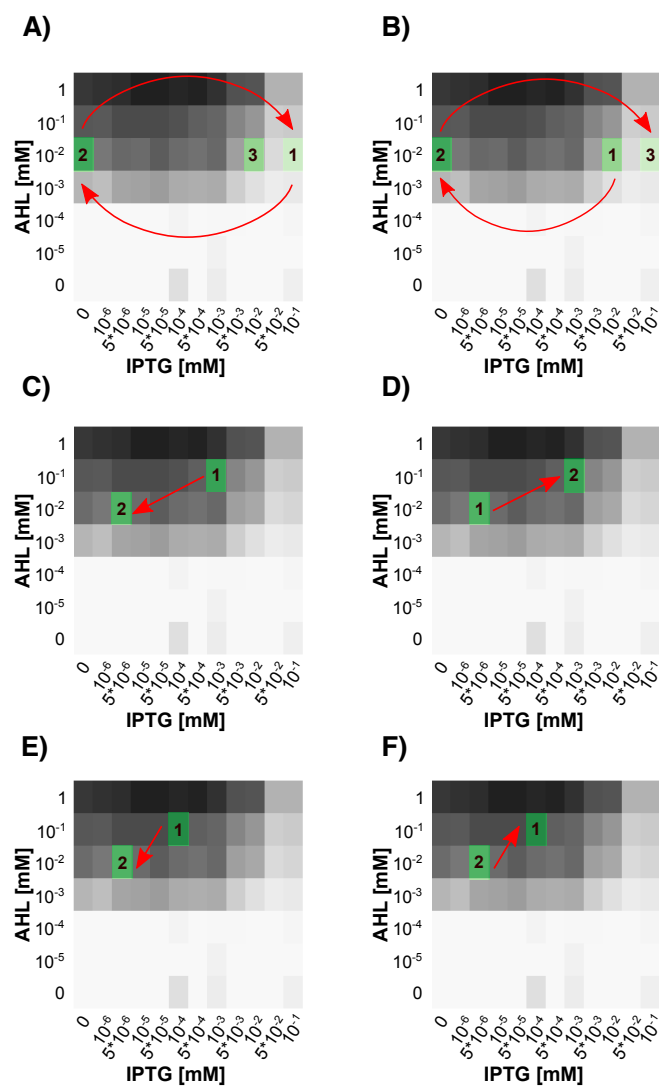
Supplementary Figure S2: Signal computation is not achieved without anti- σ . GFP expression profile, for the system lacking the anti- σ gene (MG1655 transformed with pLuSb and pVRb_ssrA plasmids), at the indicated time points post-treatment with the indicated concentrations of AHL and IPTG. Data are averages of three independent experiments. GFP values are shown as a heatmap of scaled value across the entire dynamical range of expression levels.



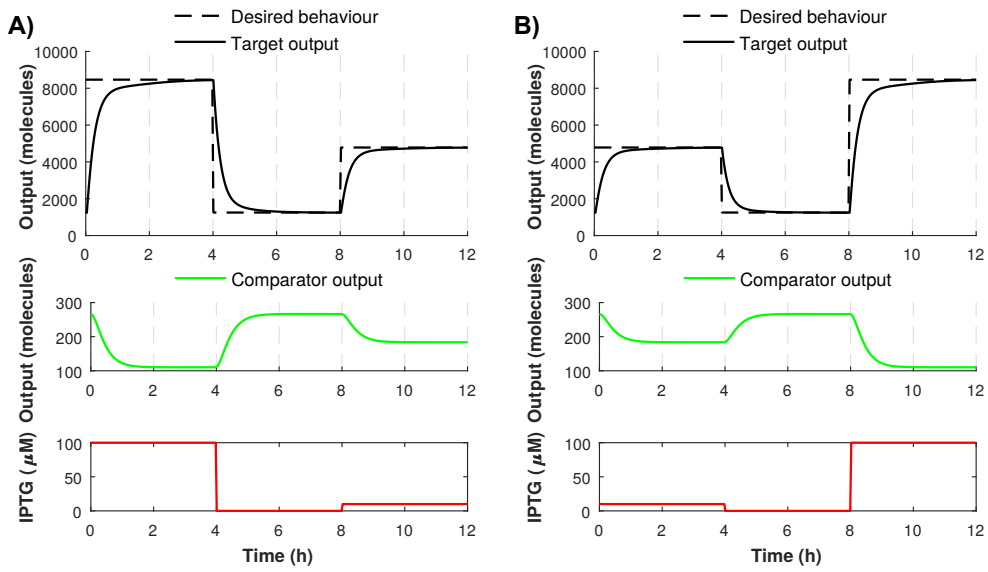
Supplementary Figure S3: Model simulation steady-state error, relative to wide-range characterisation data. Percentage absolute error between the model predictions (Figure 1-C) and the wide-range characterisation (Figure 1-B) are plotted at the indicated time points as heat maps. Data from the wide-range characterisation were filtered as described in Section S4 prior to computation of the error, so that the model predictions were directly comparable to the data used for parameter identification. Data points for AHL $\leq 10^{-4}$ mM were set to zero for the parameter identification: the (normalised) error was not computed for these values of AHL input, since it would have been infinitely large, and consequently this region is coloured white.



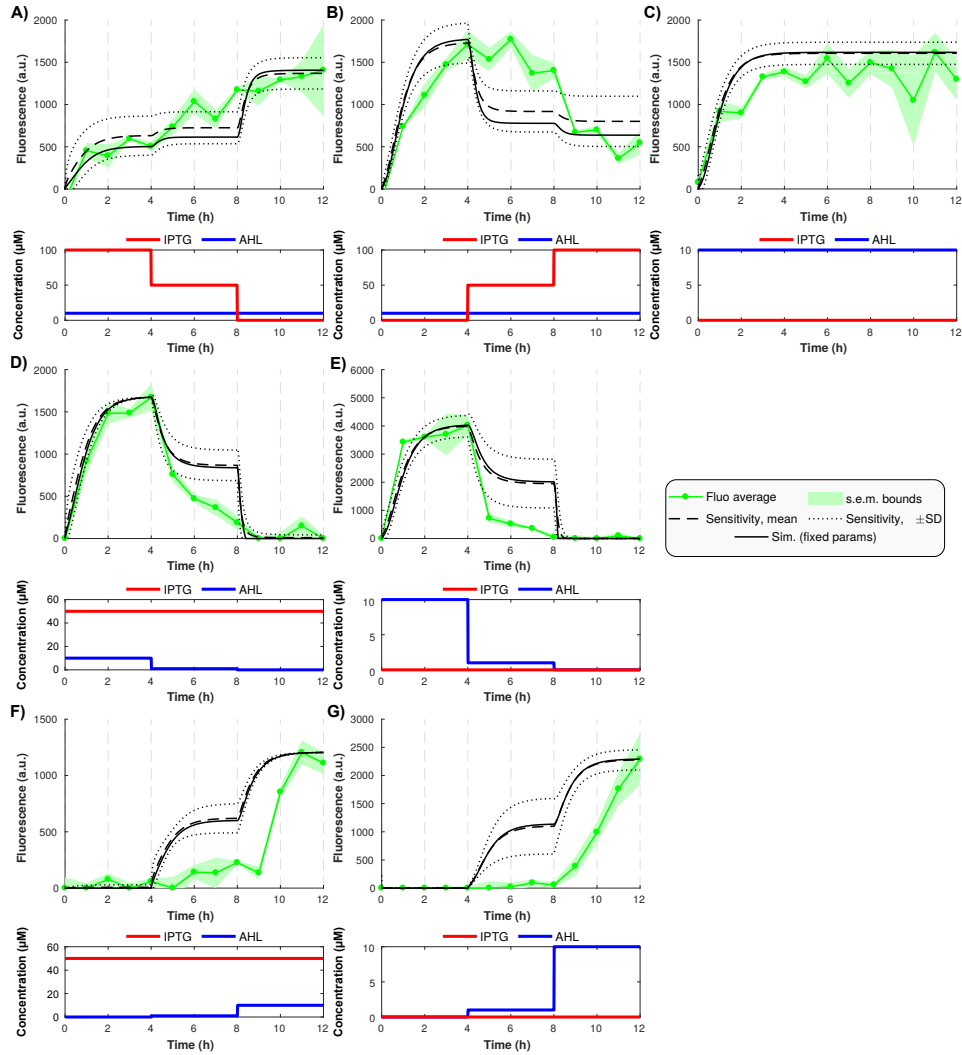
Supplementary Figure S4: Combination of concentrations used in experiments from Figure 2 (Main Matter). **A–G)** Combination of concentrations used in experiment from Figure 2 (Main Matter) mapped on the 4h heatmap from Figure 1 (Main Matter).



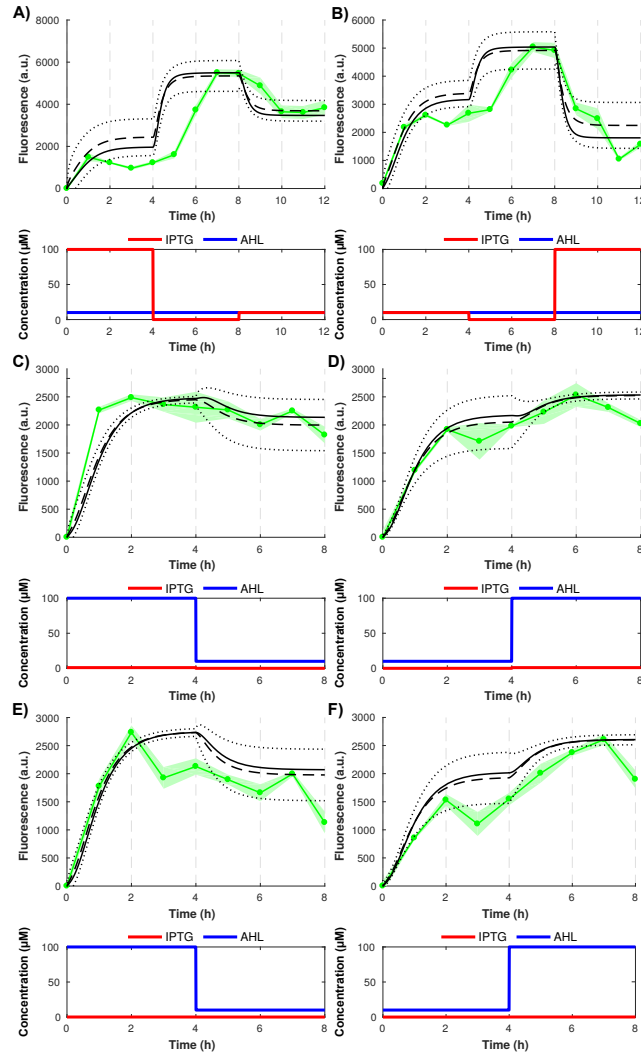
Supplementary Figure S5: Combination of concentrations used in experiments from Figure 3 (Main Matter). **A–F)** Combination of concentrations used in experiment from Figure 3 (Main Matter) mapped on the 4h heatmap from Figure 1 (Main Matter).



Supplementary Figure S6: Further *in-silico* experiments of the coupled comparator-target consortium. **A)** and **B)** show *in-silico* experiments our proposed controller consortium (Figure 4), using the IPTG input signals shown in Figure 3A and Figure 3B. The desired multi-step output is plotted in the top panels as a dashed line; the actual target output tracking this desired signal, as controlled by the computation module, is plotted as a solid black line. The central panel indicates the actual comparator output over time (green). Finally, the lower panel shows that actual IPTG reference signals corresponding to those in Figure 3A (**A**), and Figure 3B (**B**), that are fed to the comparator module in order to signal the desired response.



Supplementary Figure S7: Computational module model sensitivity analysis corresponding to input signals shown in Figure 2. In each panel, the time-lapse data are plotted as green lines, with sampling points indicated by circles, and the filled green region indicating corresponding s.e.m. over the experiments. Solid black lines indicate the baseline model output, using our final version of the fitted parameters (Table S6), as plotted in Figure 2. The dashed lines show the mean of 7000 Monte-Carlo simulations (per each condition), with each simulation using a perturbed set of parameters; surrounding dotted lines indicate the corresponding region of \pm SD. In each realisation of the Monte-Carlo simulations, the seven parameters that we had optimised by fitting to wide-range characterisation data were perturbed and the remaining parameters were kept constant. Perturbed parameters' values were chosen from a Normal distribution centred on the fitted value (Table S6) with standard deviation of 20% of that value.



Supplementary Figure S8: Computational module model sensitivity analysis corresponding to input signals shown in Figure 3. In each panel, the time-lapse data are plotted as green lines, with sampling points indicated by circles, and the filled green region indicating corresponding s.e.m. over the experiments. Solid black lines indicate the baseline model output, using our final version of the fitted parameters (Table S6), as plotted in Figure 3. The dashed lines show the mean of 7000 Monte-Carlo simulations (per each condition), with each simulation using a perturbed set of parameters; surrounding dotted lines indicate the corresponding region of \pm SD. In each realisation of the Monte-Carlo simulations, the seven parameters that we had optimised by fitting to wide-range characterisation data were perturbed and the remaining parameters were kept constant. Perturbed parameters' values were chosen from a Normal distribution centred on the fitted value (Table S6) with standard deviation of 20% of that value.

Plasmid	Promoter/genes	Replication origin	Selection	Source
pLuSb	Nter -6xHis-HRV-3Csite-HMNETDP(linker)- σ 20_992-AANDENYALAA(ssrA)- Cter expressed from the lux promoter; LuxR expressed from a constitutive promoter	p15A	Chloramphenicol	This study
pLacASb-Flag	Nter -Anti- σ 20_992-AANDENYALAA(ssrA)-Flag- Cter expressed from the lacUV5 promoter; LacI expressed from the lacI promoter	pBR322	Ampicillin	This study
pVRb-ssrA	Nter -sfGFP-AANDENYALAA(ssrA)- Cter expressed from the 20_992 promoter (σ 20_992 responsive)	pSC101	Kanamycin	This study

Supplementary Table S1: Plasmids used in this study.

3h

		Means											
		IPTG											
		0	1 nM	5 nM	10 nM	50 nM	100 nM	500 nM	1 μM	5 μM	10 μM	50 μM	100 μM
AHL	0 nM	0.0	0.0	0.0	0.0	0.0	28983.1	0.0	15303.7	0.0	0.0	0.0	9751.1
	10 nM	0.0	0.0	0.0	0.0	0.0	1026.6	0.0	11101.7	0.0	0.0	17.6	0.0
	100 nM	0.0	0.0	293.7	474.6	677.2	9300.2	1797.5	6343.4	5627.4	4190.6	3855.7	7139.3
	1000 nM	54708.4	47243.1	58014.6	61731.9	61868.6	56108.7	52455.3	49046.6	38123.6	26158.2	16676.8	20813.9
	10 μM	90574.9	74233.9	80222.7	89364.7	95957.8	90064.5	82142.3	78149.1	62128.1	58742.2	32567.1	33928.0
	100 μM	101364.0	89709.1	105300.3	104549.3	104964.5	100579.3	87586.2	85914.9	73552.1	73138.4	41226.6	43010.0
	1000 μM	128450.1	121477.8	132212.8	147044.3	146186.6	136736.7	134099.0	120736.2	104212.1	114062.1	65263.8	67441.8

		SEMs											
		IPTG											
		0	1 nM	5 nM	10 nM	50 nM	100 nM	500 nM	1 μM	5 μM	10 μM	50 μM	100 μM
AHL	0 nM	316.4	751.6	181.3	319.3	75.5	19097.5	806.2	11703.2	996.8	410.6	437.9	8315.7
	10 nM	206.9	465.2	292.2	107.4	116.7	5754.9	620.5	12149.2	544.6	597.4	4843.9	928.3
	100 nM	2581.3	1024.1	2993.3	2559.7	2176.7	7604.5	2287.2	2034.3	5827.0	5154.3	3713.0	4445.5
	1000 nM	7775.0	7372.3	5024.8	6664.9	6722.5	4074.0	3769.5	4666.3	9004.1	8107.7	6593.9	4235.1
	10 μM	12315.6	6817.6	6519.9	2944.0	7334.8	7078.6	4984.8	10899.6	8538.0	19681.0	6905.8	4460.2
	100 μM	4902.2	10899.3	3424.3	2261.5	3351.8	6440.0	9148.3	8689.8	7494.6	20406.8	6294.5	3763.7
	1000 μM	9072.1	12397.8	6864.7	10185.6	5645.2	4338.4	16975.9	9759.9	11794.6	28292.2	7756.1	7084.4

4h

		Means											
		IPTG											
		0	1 nM	5 nM	10 nM	50 nM	100 nM	500 nM	1 μM	5 μM	10 μM	50 μM	100 μM
AHL	0 nM	0.0	0.0	0.0	0.0	0.0	22578.5	0.0	12646.2	0.0	0.0	0.0	9035.2
	10 nM	0.0	0.0	0.0	0.0	0.0	0.0	0.0	8994.1	0.0	0.0	0.0	0.0
	100 nM	0.0	0.0	0.0	0.0	0.0	6916.2	0.0	2937.0	1760.0	1060.6	1341.6	4194.4
	1000 nM	45075.8	41762.1	52974.9	54892.4	57302.2	50281.1	48297.1	49688.2	33094.6	21345.0	12840.9	15657.5
	10 μM	80229.7	74040.4	81562.3	80367.4	87154.6	80308.5	76784.7	82243.9	56087.3	52392.0	26532.5	28548.7
	100 μM	91004.6	88770.5	98525.2	97212.3	97516.6	93729.0	86281.0	82967.5	67726.1	60644.7	33363.5	34550.2
	1000 μM	107618.5	111163.0	114218.2	125281.6	126065.3	120370.7	123413.7	111590.9	93942.4	92865.0	47482.5	47222.0

		SEMs											
		IPTG											
		0	1 nM	5 nM	10 nM	50 nM	100 nM	500 nM	1 μM	5 μM	10 μM	50 μM	100 μM
AHL	0 nM	362.4	487.0	355.3	340.0	448.5	16344.6	365.2	10651.5	266.6	672.1	675.6	7181.0
	10 nM	316.1	294.9	57.4	186.6	225.1	4550.0	26.2	11317.4	127.5	692.7	3704.3	358.5
	100 nM	1504.7	519.8	2065.3	1676.7	1856.4	7101.3	1203.2	1285.6	4404.2	3797.5	3476.7	3276.9
	1000 nM	4984.7	4111.8	4754.5	5427.3	5937.9	1607.5	2890.9	1749.1	7321.9	6555.3	4174.7	2982.5
	10 μM	8392.1	1945.2	5331.0	3508.3	6649.2	5585.0	2578.9	9226.5	6484.3	16070.4	4067.7	1964.7
	100 μM	5711.4	4771.0	4965.7	3661.3	5062.7	3385.8	5230.0	2046.0	6546.4	12677.8	3527.2	1515.0
	1000 μM	10874.6	5101.8	7440.3	11235.1	5975.8	1174.0	11607.3	4650.9	9865.7	21785.0	5334.3	3214.3

5h

		Means											
		IPTG											
		0	1 nM	5 nM	10 nM	50 nM	100 nM	500 nM	1 μM	5 μM	10 μM	50 μM	100 μM
AHL	0 nM	0.0	0.0	0.0	0.0	0.0	19095.2	0.0	11030.7	0.0	0.0	0.0	8325.2
	10 nM	0.0	0.0	0.0	0.0	0.0	0.0	0.0	7761.2	0.0	0.0	0.0	0.0
	100 nM	0.0	0.0	0.0	0.0	0.0	3573.0	0.0	1576.3	410.4	0.0	0.0	2204.5
	1000 nM	37196.9	36651.6	45365.0	46586.7	47838.0	43228.4	43388.2	45574.8	29116.6	18759.0	10975.1	12943.0
	10 μM	73966.2	73557.3	78741.3	74207.5	79469.5	76909.8	74586.6	85943.9	56559.2	49079.5	26880.7	25311.1
	100 μM	82850.0	86424.1	87061.4	89079.2	89368.4	89274.5	88438.5	86787.0	69196.1	55066.2	34030.6	33353.4
	1000 μM	96657.8	102958.8	100793.1	103398.7	102888.2	104714.4	107165.5	101869.7	88877.0	71975.1	42738.8	40117.2

		SEMs											
		IPTG											
		0	1 nM	5 nM	10 nM	50 nM	100 nM	500 nM	1 μM	5 μM	10 μM	50 μM	100 μM
AHL	0 nM	385.9	492.8	318.5	403.1	390.2	15575.9	547.7	9022.4	367.1	320.8	443.0	6600.7
	10 nM	379.1	420.0	294.2	218.7	181.2	2677.7	357.9	10288.2	257.2	430.9	2312.8	562.3
	100 nM	914.8	324.0	1241.4	960.9	970.4	4584.9	1004.0	938.0	3343.7	2720.1	2325.7	2911.2
	1000 nM	1859.3	1325.9	2558.8	3433.0	2343.8	2049.3	4128.5	1382.9	5415.8	3130.9	2528.6	1792.8
	10 μM	1637.4	1873.6	3563.2	1747.0	2016.3	1716.4	3226.8	8455.1	3933.4	9931.3	3058.0	107.3
	100 μM	1457.5	1583.8	2002.4	4186.3	3325.5	2139.8	3518.8	1856.0	3943.3	4222.5	832.4	217.3
	1000 μM	4674.5	848.8	2925.2	3232.0	3869.4	5354.7	5398.5	1388.5	1912.8	4869.9	526.9	270.7

Supplementary Table S2: Absolute values and S.E.M. for the wide range characterization experiments. Absolute values and S.E.M. for the wide range characterization experiments. Data normalized by subtracting the background intensity and normalizing on the OD600 measurements. After normalization, data from three independent experiments from each time point are averaged and scaled across the full dynamical range ((measured value - min value)/(max value - min value)).

Name	Sequence
Sigma_FW	5'-ATAGGATTAATCCATGGGCAGCAGCCATCATCATCATCACAGCAGCGG-3'
Sigma_ssrA_RW	5'-ATTTAAGGATCCTCACGCTGCAAGGGCGTAATTTTCGTTCGTTTCGCTGCACTAGTCGGTTTGCGACGACGA CCGCTCAGATCTGCACC-3'
LacIASb_Vector_F	5'-AGAAGATTTTCAGCCCACCACCACCCTGAGATCC-3'
LacIASb_Vector_R	5'-TGCCTAATGGAATTCGGGATCGAGATCTCGATCCT-3'
LacIASb_Frag1_F	5'-CGAGATCTCGATCCCGAATTCATTAGGCATTAGGCACCC-3'
LacIASb_Frag1_R	5'-TTCCGGTGTGCCCATCTTTACCTCCTCTATCGCGGA-3'
LacIASb_Frag2_F	5'-ATAGAGGAGGTAAAGATGGGCACACCGGAACGT-3'
LacIASb_Frag2_R	5'-TCAGTGGTGGTGGTGGGCTGAAAATCTTCTCTCATCCGC-3'
ASb_Flag_F	5'-GACGACGATAAGATCGATTACAAGGATGACGACGATAAGTAAGGATCCAAGCTTGGCTGTTTTGGCGG-3'
ASb_Flag_R	5'-ATCCTTGTAATCTCCCTTATCGTCGTCATCCTTGTAATCCGCTGCAAGGGCGTAATTTTCGTC-3'
GFPssrA_F	5'-CTTGCAGCGTAATCCAGACCTGCAGGCATGCAAGCCTCTAGAG-3'
GFPssrA_R	5'-GGCGTAATTTTCGTTCGTTTCGCTGCTTTGTAGAGCTCATCCATGCC-3'
AntiSigma_FW	5'-TTATTCCATGGGCACACCGGAACGTTTTGTTTCATCTGGCAGATGCC-3'
AntiSigma_ssrA_RW	5'-TAGCCAAGCTTGGATCCTTACGCTGCAAGGGCGTAATTTTCGTTCGTTTCGCTGCACTAGTCTGTTC TGCTTCTTCTGCATTAATGC-3'

Supplementary Table S3: Primers used in this study.

S2 Model Derivation

In this section we describe the features and derivation of the ODE-based mathematical model of our proposed signal computation system GRN (Figure 1-a).

S2.1 Model assumptions

- We use a continuous and deterministic ordinary differential equation (ODE) model to represent the system dynamics. Reactions are represented through mass-action kinetics, and we do not explicitly account for population growth since the number of cells is kept constant throughout experiments.
- For all species in the system, we assume that the variation in plasmid copy number is not large enough to significantly affect the dynamics and can be neglected from the model.
- Diffusion of IPTG into the population is assumed to occur instantaneously (the internal concentration instantaneously reaches the desired signal reference concentration within the population when modified externally)¹².
- Similarly we assume the internal AHL concentration instantaneously assumes the externally applied concentration¹³.
- For the AHL, we assume that there is a steady equilibrium concentration of the relevant proteins (LuxR for the activation of AHL), that is sufficiently high to consider any AHL in the cell to be bound as the LuxR:AHL complex and thus act directly on the AHL responsive promoter². Possible aggregated effects of saturation and competition are subsumed under the (fitted) co-operativity coefficient of this promoter (see Section S4).
- We assume that interactions between sigma and RNA polymerase can be neglected, and therefore in the model the p20_992 promoter is driven directly by the concentration of free sigma. In other words, ancillary dynamics of the sigma factor (e.g., possible competition with endogenous sigma factors, see⁹) are aggregated in the parameters and equation of the p20_992 promoter governing transcription of GFP (Equation S20).

S2.2 Summary of dynamical variables in the full model

State variable	Description
$[M_\sigma]$	mRNA concentration for sigma factor.
$[M_{\sigma_\alpha}]$	mRNA concentration for anti-sigma.
$[M_{\text{GFP}}]$	mRNA concentration for GFP.
$[P_{\text{GFP}}]$	Mature GFP concentration.
$[\sigma_{\text{free}}]$	Concentration of free sigma factor.
$[\sigma_{\alpha,\text{free}}]$	Concentration of free anti-sigma.
$[\sigma:\sigma_\alpha]$	Concentration of the sigma:anti-sigma complex (bound sigma and anti-sigma).

Supplementary Table S4: Overview of the seven dependent variables defined in the full model. Here, for σ and σ_α , the subscript ‘free’ denotes the fact that these species are not in complex *with each other* (denoted $\sigma:\sigma_\alpha$); it is unrelated to binding with RNA polymerase, which is not considered in our model (see Section S2.1, ‘Model assumptions’).

S2.3 Reactions considered in the full model

Reaction	Description
$\frac{H^+([A])}{\rightarrow} M_\sigma$	Transcription of sigma (σ) mRNA.
$\frac{H^+([I])}{\rightarrow} M_{\sigma_\alpha}$	Transcription of anti-sigma (σ_α) mRNA.
$\frac{H^+([\sigma])}{\rightarrow} M_{\text{GFP}}$	Transcription of GFP mRNA.
$M_\sigma \xrightarrow{\gamma_{M_\sigma}} \emptyset$	Degradation of σ mRNA.
$M_{\sigma_\alpha} \xrightarrow{\gamma_{M_{\sigma_\alpha}}} \emptyset$	Degradation of σ_α mRNA.
$M_{\text{GFP}} \xrightarrow{\gamma_{M_{\text{GFP}}}} \emptyset$	Degradation of GFP mRNA.
$M_\sigma \xrightarrow{k_\sigma} \sigma_{\text{free}}$	Translation of σ from its mRNA.
$M_{\sigma_\alpha} \xrightarrow{k_{\sigma_\alpha}} \sigma_{\alpha,\text{free}}$	Translation of σ_α from its mRNA.
$M_{\text{GFP}} \xrightarrow{k_{\text{GFP}}} P_{\text{GFP}}$	Translation and maturation of GFP.
$\sigma_{\text{free}} \xrightarrow{f(X)} \emptyset$	Degradation of σ (ssrA tagged).
$\sigma_{\alpha,\text{free}} \xrightarrow{f(X)} \emptyset$	Degradation of σ_α (ssrA tagged).
$P_{\text{GFP}} \xrightarrow{f(X)} \emptyset$	Degradation of mature GFP (ssrA tagged).
$\sigma_{\text{free}} \xrightarrow{\gamma} \emptyset$	Dilution of σ due to cell division.
$\sigma_{\alpha,\text{free}} \xrightarrow{\gamma} \emptyset$	Dilution of σ_α due to cell division.
$P_{\text{GFP}} \xrightarrow{\gamma} \emptyset$	Dilution of mature GFP due to cell division.
$\sigma_{\text{free}} + \sigma_{\alpha,\text{free}} \xrightarrow{k_{\sigma:\sigma_\alpha}^+} \sigma:\sigma_\alpha$	$\sigma:\sigma_\alpha$ complex formation from one σ and one σ_α .
$\sigma:\sigma_\alpha \xrightarrow{k_{\sigma:\sigma_\alpha}^-} \sigma_{\text{free}} + \sigma_{\alpha,\text{free}}$	Dissociation of one $\sigma:\sigma_\alpha$ complex into one σ and one σ_α .
$\sigma:\sigma_\alpha \xrightarrow{f(X)} \emptyset$	Degradation of one $\sigma:\sigma_\alpha$ complex.
$\sigma:\sigma_\alpha \xrightarrow{\gamma} \emptyset$	Dilution of $\sigma:\sigma_\alpha$ complex due to cell division.
$\sigma_{\text{total}} = \sigma_{\text{free}} + \sigma:\sigma_\alpha$	Conservation of σ : total sigma is the sum of concentrations in its free and bound forms.
$\sigma_{\alpha,\text{total}} = \sigma_{\alpha,\text{free}} + \sigma:\sigma_\alpha$	Conservation of σ_α : total anti-sigma is the sum of concentrations in its free and bound forms.

Supplementary Table S5: A summary of all major reactions considered in our full model of the $\sigma:\sigma_\alpha$ system, before simplification of the equations.

S2.4 Dynamics of the full model

We begin by specifying the dynamics of intracellular mRNA through a saturating Hill curve parametrised by an input concentration of some transcription factor, a half-maximal activation concentration, and a Hill coefficient^{1,4,6,8}. The general form of the dynamical equations for an mRNA species M_i is therefore defined as

$$\frac{d[M_i]}{dt} = \alpha_{0,i} + \alpha_{1,i}H(P_x) - \gamma_{M_i}[M_i], \quad (\text{S1})$$

where $[X]$ denotes the concentration of species X , γ_i is the rate of mRNA degradation, $\alpha_{0,i}$ and $\alpha_{1,i}$ are the basal and maximal transcription rates and $H(P_x)$ is an activation, or inhibition, of the promoter regulated by the transcription factor P_x . The function regulating activation of the promoter for transcription of mRNA species M_i by species P_x is

$$H(P_x) = H_+(P_x) = \frac{[P_x]^{n_x}}{K_x^{n_x} + [P_x]^{n_x}}, \quad (\text{S2})$$

and likewise for inactivation/inhibition by species P_x

$$H(P_x) = H_-(P_x) = \frac{K_x^{n_x}}{K_x^{n_x} + [P_x]^{n_x}}, \quad (\text{S3})$$

where α_i is the maximal transcription rate, K_x is the microscopic dissociation constant, and n_x is a Hill coefficient defining cooperativity of binding to the promoter (steepness of the response curve).

mRNA dynamics

The transcription of sigma factor mRNA, M_σ , is determined by the activity of the pLux promoter, which is activated by the presence of AHL (whose concentration is $[A]$):

$$\frac{d[M_\sigma]}{dt} = \alpha_{0,\sigma} + \frac{\alpha_{1,\sigma}[A]^{n_A}}{K_A^{n_A} + [A]^{n_A}} - \gamma_{M_\sigma}[M_\sigma]. \quad (\text{S4})$$

Transcription of the corresponding anti-sigma mRNA, $M_{\sigma\alpha}$, is determined by the intracellular concentration of IPTG, I :

$$\frac{d[M_{\sigma\alpha}]}{dt} = \alpha_{0,\sigma\alpha} + \frac{\alpha_{1,\sigma\alpha}[I]^{n_I}}{K_I^{n_I} + [I]^{n_I}} - \gamma_{M_{\sigma\alpha}}[M_{\sigma\alpha}]. \quad (\text{S5})$$

Finally, the transcription of GFP mRNA is driven by the p_{20_992} promoter (see¹¹). This promoter's activity is regulated directly by our sigma factor:

$$\frac{d[M_{\text{GFP}}]}{dt} = \alpha_{0,\text{GFP}} + \frac{\alpha_{1,\text{GFP}}[\sigma_{\text{free}}]^{n_\sigma}}{K_\sigma^{n_\sigma} + [\sigma_{\text{free}}]^{n_\sigma}} - \gamma_{M_{\text{GFP}}}[M_{\text{GFP}}]. \quad (\text{S6})$$

Translation dynamics

Dynamics of proteins in then system consist of linear first order reactions, similar to typical models in the literature (e.g.,^{4,6,8}). We explicitly account for different kinetics for all interactions, by including these as unique parameters unless otherwise specified.

In general, a protein species P_i evolves in time relative to its corresponding mRNA quantity M_i as

$$\frac{d[P_i]}{dt} = k_i[M_i] - \gamma_{P_i}[P_i], \quad (\text{S7})$$

where k_i is the forward rate constant for translation of mRNA M_i to protein P_i , and γ_{P_i} is the rate of first order degradation of P_i . In our model, we consider enzymatic degradation through the *ssrA* tag mechanism to be the dominant form of degradation for all P_i ; for this, we later include an extra term for each species and therefore here $\gamma_{P_i} = \gamma$ i.e., a constant dilution for all protein species (discussed in the next section).

ssrA-tagged proteins: enzymatic degradation

In order to implement enzymatic degradation of *ssrA* tagged proteins (free and bound sigma and anti-sigma, GFP), we define a nonlinear *ssrA* tag based degradation rate, $f(X)$, of the form previously used in^{3,10,12} among others:

$$f(X) = \frac{\gamma_D}{c_e + X}, \quad (\text{S8})$$

where γ_D (molecules min^{-1}) defines the maximal rate of enzymatic degradation, c_e (molecules) defines the half-activation threshold of the degradation, and

$$X = [\sigma_{\text{free}}] + [\sigma_{\alpha,\text{free}}] + [\sigma:\sigma_{\alpha}] + [\text{GFP}] \quad (\text{S9})$$

is the total number of *ssrA* tagged proteins present in the system (Table S4). The value of X is dynamic and so this equation implements a form of competition between available *ssrA* tag selecting proteases, since there is physically a limit on the number of available proteases.

Sigma factor

Dynamics of the concentration of the free sigma factor, σ_{free} , are defined as

$$\begin{aligned} \frac{d[\sigma_{\text{free}}]}{dt} = & \overbrace{k_{\sigma}[M_{\sigma}]}^{(i)} - \overbrace{k_{\sigma:\sigma_{\alpha}}^{+}[\sigma_{\text{free}}][\sigma_{\alpha,\text{free}}]}^{(ii)} + \overbrace{k_{\sigma:\sigma_{\alpha}}^{-}[\sigma:\sigma_{\alpha}]}^{(iii)} \\ & - \underbrace{f(X)[\sigma_{\text{free}}]}_{(iv)} - \underbrace{\gamma[\sigma_{\text{free}}]}_{(v)}. \end{aligned} \quad (\text{S10})$$

The various components of Equation S10 represent a number of chemical interactions, as follows:

- (i) generation of σ_{free} with translation rate k_{σ} , governed by the concentration of its mRNA;
- (ii) protein-protein interaction (association) representing the loss of σ_{free} through reversible binding, at rate $k_{\sigma:\sigma_{\alpha}}^{+}$, with the anti-sigma $\sigma_{\alpha,\text{free}}$ to form the complex $\sigma:\sigma_{\alpha}$;
- (iii) increase in σ_{free} resulting from dissociation of the $\sigma:\sigma_{\alpha}$ complex, with dissociation rate $k_{\sigma:\sigma_{\alpha}}^{-}$;
- (iv) degradation of σ_{free} via ssrA tag mechanism;
- (v) dilution of σ_{free} through cell division.

Anti-sigma

The dynamics of the free anti-sigma, denoted by $\sigma_{\alpha,\text{free}}$, following a similar process as those of the sigma, are defined in Equation S11 below:

$$\begin{aligned} \frac{d[\sigma_{\alpha,\text{free}}]}{dt} = & \overbrace{k_{\sigma_{\alpha}}[M_{\sigma_{\alpha}}]}^{(i)} - \overbrace{k_{\sigma:\sigma_{\alpha}}^{+}[\sigma_{\text{free}}][\sigma_{\alpha,\text{free}}]}^{(ii)} + \overbrace{k_{\sigma:\sigma_{\alpha}}^{-}[\sigma:\sigma_{\alpha}]}^{(iii)} \\ & - \underbrace{f(X)[\sigma_{\alpha,\text{free}}]}_{(iv)} - \underbrace{\gamma[\sigma_{\alpha,\text{free}}]}_{(v)}. \end{aligned} \quad (\text{S11})$$

with

- (i) the translation of $\sigma_{\alpha,\text{free}}$ from its mRNA, at rate $k_{\sigma_{\alpha}}$;
- (ii) loss of $\sigma_{\alpha,\text{free}}$ as it reversibly binds to σ_{free} with rate $k_{\sigma:\sigma_{\alpha}}^{+}$, forming the $\sigma:\sigma_{\alpha}$ complex;
- (iii) increase in free $\sigma_{\alpha,\text{free}}$ from dissociation of $\sigma:\sigma_{\alpha}$ at rate $k_{\sigma:\sigma_{\alpha}}^{-}$;
- (iv) degradation of $\sigma_{\alpha,\text{free}}$ via ssrA tag mechanism;
- (v) dilution of $\sigma_{\alpha,\text{free}}$ through cell division.

The term (iv) was initially specified in a modified form

$$\gamma_{\text{Flag}} f(X)[\sigma_{\alpha,\text{free}}],$$

where $\gamma_{\text{Flag}} < 1$ represents a loss of enzymatic degradation efficiency resulting from the presence of the Flag tag. However preliminary model analysis, via both manual parameter adjustment and global optimisation, indicated that the system output did not conform to observed measurements on inclusion of the factor γ_{Flag} . This scaling was therefore not included in the final model.

Sigma:anti-sigma complex

We denote the sigma:anti-sigma complex by $\sigma:\sigma_{\alpha}$. Its dynamics consist of the formation, dissociation, and degradation (independent of the individual

degradation of its constituents) of the complex, as follows:

$$\frac{d[\sigma:\sigma_\alpha]}{dt} = \underbrace{k_{\sigma:\sigma_\alpha}^+ [\sigma_{\text{free}}] [\sigma_{\alpha,\text{free}}]}_{(i)} - \underbrace{k_{\sigma:\sigma_\alpha}^- [\sigma:\sigma_\alpha]}_{(ii)} - \underbrace{f(X) [\sigma:\sigma_\alpha]}_{(iii)} - \underbrace{\gamma [\sigma:\sigma_\alpha]}_{(iv)}, \quad (\text{S12})$$

with

- (i) the interaction between σ and σ_α with binding (association) at rate $k_{\sigma:\sigma_\alpha}^+$;
- (ii) the dissociation, at rate $k_{\sigma:\sigma_\alpha}^-$, of the complex $\sigma:\sigma_\alpha$;
- (iii) the enzymatic degradation of sigma/anti-sigma bound in complex;
- (iv) dilution of the complex concentration resulting from cell division.

Output

Production of the GFP from its mRNA is straightforward:

$$\frac{d[P_{\text{GFP}}]}{dt} = k_{\text{GFP}} [M_{\text{GFP}}] - f(X) [P_{\text{GFP}}] - \gamma [P_{\text{GFP}}]. \quad (\text{S13})$$

The GFP is translated with rate k_{GFP} and diluted at rate γ . Furthermore, since it is also tagged for degradation, we include the enzymatic degradation term $f(X)$.

S3 Model simplification

In order to reduce the number of parameters required for subsequent model identification and parameter fitting, we simplified the original model. Through initial simulations, we determined that it was necessary to include the full dynamics of the complex formation and dissociation as these would be slow relative to the dynamics of the rest of the system. However, the separate dynamics of the mRNA and proteins could be merged.

If we consider the dynamics of mRNA transcription as being fast compared to the translation process, we can extend the quasi-steady-state approximation to the mRNA (Equations S4–S6) and the protein dynamics (Equations S10,S11 and S13). We consider mRNA dynamics to effectively be at steady state so that

$$\begin{aligned}\frac{d[M_\sigma]}{dt} &\approx 0, \\ \frac{d[M_{\sigma\alpha}]}{dt} &\approx 0, \\ \frac{d[M_{\text{GFP}}]}{dt} &\approx 0.\end{aligned}$$

Consequently, from Equations S4–S6, we obtain the following relationships for the mRNA concentrations:

$$[M_{\text{GFP}}] = \frac{1}{\gamma_{M\text{GFP}}} \left(\alpha_{0,\text{GFP}} + \frac{\alpha_{1,\text{GFP}}[\sigma_{\text{free}}]^{n_\sigma}}{K_\sigma^{n_\sigma} + [\sigma_{\text{free}}]^{n_\sigma}} \right), \quad (\text{S14})$$

$$[M_\sigma] = \frac{1}{\gamma_{M\sigma}} \left(\alpha_{0,\sigma} + \frac{\alpha_{1,\sigma}[A]^{n_A}}{K_A^{n_A} + [A]^{n_A}} \right), \quad (\text{S15})$$

$$[M_{\sigma\alpha}] = \frac{1}{\gamma_{M\sigma\alpha}} \left(\alpha_{0,\sigma\alpha} + \frac{\alpha_{1,\sigma\alpha}[I]^{n_I}}{K_I^{n_I} + [I]^{n_I}} \right). \quad (\text{S16})$$

We can substitute Equations S14–S16 into the relevant protein dynamics (Equations S10,S11 and S13) to obtain the following equations for the simplified GFP dynamics

$$\frac{d[P_{\text{GFP}}]}{dt} = \frac{k_{\text{GFP}}}{\gamma_{M\text{GFP}}} \left(\alpha_{0,\text{GFP}} + \frac{\alpha_{1,\text{GFP}}[\sigma_{\text{free}}]^{n_\sigma}}{K_\sigma^{n_\sigma} + [\sigma_{\text{free}}]^{n_\sigma}} \right) - f(X)[P_{\text{GFP}}] - \gamma_{P\text{GFP}}[P_{\text{GFP}}]. \quad (\text{S17})$$

The sigma and anti-sigma can be treated in a similar manner:

$$\begin{aligned}\frac{d[\sigma_{\text{free}}]}{dt} &= \frac{k_\sigma}{\gamma_{M\sigma}} \left(\alpha_{0,\sigma} + \frac{\alpha_{1,\sigma}[A]^{n_A}}{K_A^{n_A} + [A]^{n_A}} \right) - k_{\sigma:\sigma_\alpha}^+ [\sigma_{\text{free}}][\sigma_{\alpha,\text{free}}] \\ &\quad + k_{\sigma:\sigma_\alpha}^- [\sigma:\sigma_\alpha] - f(X)[\sigma_{\text{free}}] - \gamma_\sigma[\sigma_{\text{free}}], \quad (\text{S18})\end{aligned}$$

$$\begin{aligned} \frac{d[\sigma_{\alpha,\text{free}}]}{dt} = & \frac{k_{\sigma\alpha}}{\gamma_{M\sigma\alpha}} \left(\alpha_{0,\sigma\alpha} + \frac{\alpha_{1,\sigma\alpha}[I]^{n_I}}{K_I^{n_I} + [I]^{n_I}} \right) - k_{\sigma:\sigma\alpha}^+ [\sigma_{\text{free}}][\sigma_{\alpha,\text{free}}] \\ & + k_{\sigma:\sigma\alpha}^- [\sigma:\sigma\alpha] - f(X)[\sigma_{\alpha,\text{free}}] - \gamma_{\sigma\alpha}[\sigma_{\alpha,\text{free}}]. \end{aligned} \quad (\text{S19})$$

Finally, in order to aid the identification process, we combine parameters related to transcription, translation, and mRNA degradation by introducing the variables

$$\begin{aligned} \chi_{0,i} &= \frac{k_i \alpha_{0,i}}{\gamma_{Mi}} \\ \chi_{1,i} &= \frac{k_i \alpha_{1,i}}{\gamma_{Mi}}, \end{aligned}$$

where the subscript i indicates a particular chemical species (GFP, σ , and σ_α). Finally, introducing the lumped parameters $\chi_{0,i}$ and χ_i into Equations S17, S18 and S19, gives us the final form of the protein dynamics as follows:

$$\frac{d[P_{\text{GFP}}]}{dt} = \chi_{0,\text{GFP}} + \frac{\chi_{1,\text{GFP}}[\sigma_{\text{free}}]^{n_\sigma}}{K_\sigma^{n_\sigma} + [\sigma_{\text{free}}]^{n_\sigma}} - f(X)[P_{\text{GFP}}] - \gamma_{P_{\text{GFP}}}[P_{\text{GFP}}], \quad (\text{S20})$$

$$\begin{aligned} \frac{d[\sigma_{\text{free}}]}{dt} = & \chi_{0,\sigma} + \frac{\chi_{1,\sigma}[A]^{n_A}}{K_A^{n_A} + [A]^{n_A}} - k_{\sigma:\sigma\alpha}^+ [\sigma_{\text{free}}][\sigma_{\alpha,\text{free}}] \\ & + k_{\sigma:\sigma\alpha}^- [\sigma:\sigma\alpha] - f(X)[\sigma_{\text{free}}] - \gamma_\sigma[\sigma_{\text{free}}], \end{aligned} \quad (\text{S21})$$

$$\begin{aligned} \frac{d[\sigma_{\alpha,\text{free}}]}{dt} = & \chi_{0,\sigma\alpha} + \frac{\chi_{1,\sigma\alpha}[I]^{n_I}}{K_I^{n_I} + [I]^{n_I}} - k_{\sigma:\sigma\alpha}^+ [\sigma_{\text{free}}][\sigma_{\alpha,\text{free}}] \\ & + k_{\sigma:\sigma\alpha}^- [\sigma:\sigma\alpha] - f(X)[\sigma_{\alpha,\text{free}}] - \gamma_{\sigma\alpha}[\sigma_{\alpha,\text{free}}], \end{aligned} \quad (\text{S22})$$

and complex dynamics

$$\frac{d[\sigma:\sigma\alpha]}{dt} = k_{\sigma:\sigma\alpha}^+ [\sigma_{\text{free}}][\sigma_{\alpha,\text{free}}] - k_{\sigma:\sigma\alpha}^- [\sigma:\sigma\alpha] - f(X)[\sigma:\sigma\alpha] - \gamma[\sigma:\sigma\alpha]. \quad (\text{S23})$$

Equations S20–S23 comprise the fully simplified system used for parameter identification and system simulation.

S4 Parameter identification

Based on the wide-range characterisation of the reference comparator module (steady-state data indicated in the main material, Figure 1-B), we performed an identification to obtain an estimate of our unknown parameters. MATLAB 2016b¹ was used for all simulations.

The identification of unknown parameters was performed using the particle swarm optimisation routine built into MATLAB. This optimisation algorithm is a population-based technique, similar to a genetic algorithm, that attempts to find a globally optimal solution to an optimisation problem, therefore generating a set of parameters that are the most likely to correspond to the best possible solution for a given set of problem constraints.

Particle swarm optimization experiments were performed only on the data obtained at the 4-hour time point, as at this point we determined the experimental system had converged to a steady state response. Prior to optimisation, the data were filtered using a 2D Gaussian filter (MATLAB's `imgaussfit()` routine, with $\sigma = 1.0$); the full range of points obtained across all IPTG and AHL inputs were used for the fitting. The objective function used for global optimisation computed the sum of squared errors between all model and data points, where each point's contribution to the total objective error was weighted according to the experimentally measured S.E.M. at that point (Supplementary Table S2).

We performed an exhaustive set of optimization experiments by changing weights in the objective function, selecting those parameter values that were observed heuristically to better match the time lapse experimental data.

Final values of optimised parameters obtained from the wide-range characterisation are shown in Table S6.

¹MATLAB Release 2016b, The MathWorks, Inc., Natick, Massachusetts, United States.

Parameter	Description	Baseline value	Optimised value	Source (baseline)
$\chi_{0,i}$	Basal transcription rate for mRNA species i .	54 molecules min ⁻¹		12
$\chi_{1,i}$	Maximal transcription rate for mRNA species i .	1080 molecules min ⁻¹		12
γ_{Mi}	Rate of decay of mRNA species i .	0.54 min ⁻¹		12
$\gamma_{M_{GFP}}$	Rate of decay of GFP mRNA.	0.288 min ⁻¹		7
K_{σ} **	Microscopic dissociation constant for σ -regulated promoter.	3000 molecules	1.98×10^4 molecules	*
K_I **	Microscopic dissociation constant for IPTG-regulated promoter.	35 μ M	90 μ M	12
K_A	Microscopic dissociation constant for AHL-regulated promoter.	10 nM		2
n_{σ} **	Hill coefficient for σ -regulated promoter.	2	1.93	1
n_A **	Hill coefficient for AHL-regulated promoter.	2	0.31	1
n_I **	Hill coefficient for IPTG-regulated promoter.	2	0.46	1
k_i	Rate of translation of protein species i from its mRNA.	81 min ⁻¹		12
k_{GFP}	Total rate of translation and maturation of GFP.	1.797 min ⁻¹		7
γ_{Pi}	Rate of dilution of protein species i .	0.0277 min ⁻¹		25 min generation time.
γ_D **	Maximal rate of degradation through <i>ssrA</i> tags.	1080 molecules min ⁻¹	701.2 molecules min ⁻¹	12
c_e **	Half-maximal concentration for kinetics of <i>ssrA</i> tag based degradation.	0.1 molecules	0.01 molecules	12
$k_{\sigma:\sigma_{\alpha}}^+$	Rate of complex formation (association of σ and σ_{α})	0.018 min ⁻¹ molecules ⁻¹		12
$k_{\sigma:\sigma_{\alpha}}^-$	Rate of complex dissociation ($\sigma:\sigma_{\alpha}$ into its constituents)	0.00018 min ⁻¹		12

Supplementary Table S6: Kinetic parameters of the GRN model and their meaning, along with baseline values (used where a parameter was not being optimised/fitted to experimental data), the final optimised value after identification procedure described in Section S4 and sources for the baseline parameter values. N.b., the units for K_A and K_I are specified as μ M corresponding to the experimental AHL and IPTG input signals used in the study; in contrast K_{σ} is specified in units of molecules since this promoter is directly activated by σ , a state variable that is itself specified in units of molecules. All parameter values are quoted as essentially being ‘per cell’, on average, in our aggregate model i.e., rates implicitly incorporate an assumed effect of a plasmid copy number $\gg 1$.

*The initial value of K_{σ} was estimated via a preliminary model identification on the data presented in¹¹.

**This subset of the parameters were optimised according to the identification procedure described in Section S4.

S5 Cellular consortium and comparator model

In order to validate the performance of our signal computation module, as well as test the fitted parameters (Table S6), we integrated it into a more complex system. This ‘extended model’ consisted of the proposed signal computation module acting as a reference comparator in a negative feedback control loop on a target population of cells, as proposed in⁵.

The target cells’ GRN was modelled as follows:

$$\frac{d[C]}{dt} = \chi_{0,C} + \frac{\chi_{1,C}[Q_t]^{n_Q}}{K_Q^{n_Q} + [Q_t]^{n_Q}} - g(X)[C] - \gamma[C], \quad (\text{S24})$$

$$\frac{d[D]}{dt} = \chi_{0,D} + \frac{\chi_{1,D}K_C^{n_C}}{K_C^{n_C} + [C]^{n_C}} - g(X)[D] - \gamma[D], \quad (\text{S25})$$

where the parameters have the same meaning as those in the comparator GRN discussed in the previous sections: all χ and γ take the same values as in the comparator GRN ($\chi_{0,i} = 54$ molecules min^{-1} ; $\chi_{1,i} = 1080$ molecules min^{-1} ; $\gamma = 0.0277$ min^{-1}), while the target GRN specific parameters $n_Q = n_C = 2$, $K_Q = 9$ molecules, and $K_C = 900$ molecules. The nonlinear enzymatic degradation function $g(X)$ is analogous to $f(X)$ (Equation S8), and is defined as

$$g(X) = \frac{\gamma_D}{c_e + X}, \quad (\text{S26})$$

where in the target GRN

$$X = [C] + [D], \quad (\text{S27})$$

and where $\gamma_D = 701.2$ molecules min^{-1} and $c_e = 0.01$ molecules are defined as above in S26, with the same values as those used in the comparator GRN.

In the extended model, we consider only a single external input, the IPTG corresponding to our external reference signal. AHL ($[A]$) that is sensed by the reference comparator is generated from the target GRN; likewise, the reference comparator generates an orthogonal quorum molecule $[Q]$ that is sensed by the target population. The equations for dynamics of the AHL molecule $[A]$ concentration, for the comparator GRN (subscript c), the target GRN (subscript t) and external to the cells (subscript e), are defined as

$$\frac{d[A_c]}{dt} = \nu_A [P_{\text{GFP}}] + \eta([A_e] - [A_c]) - \gamma_{A,i}[A_c], \quad (\text{S28})$$

$$\frac{d[A_t]}{dt} = \eta([A_e] - [A_t]) - \gamma_{A,i}[A_t], \quad (\text{S29})$$

$$\frac{\partial [A_e]}{\partial t} = \eta([A_c] - [A_e]) + \eta([A_t] - [A_e]) - \gamma_{A,e}[A_e] + \Theta \nabla^2 [A_e]; \quad (\text{S30})$$

Note that in this extension of the model, the static AHL input $[A]$ to the comparator GRN (in Equation S18, for example) is replaced by the dynamical variable $[A_c]$. Likewise the dynamics of Q , the signalling pathway from the comparator to the target, are defined as:

$$\frac{d[Q_c]}{dt} = \eta([Q_e] - [Q_c]) - \gamma_{Q,i}[Q_c], \quad (\text{S31})$$

$$\frac{d[Q_t]}{dt} = \nu_Q[D] + \eta([Q_e] - [Q_t]) - \gamma_{Q,i}[Q_t], \quad (\text{S32})$$

$$\frac{\partial[Q_e]}{\partial t} = \eta([Q_c] - [Q_e]) + \eta([Q_t] - [Q_e]) - \gamma_{Q,e}[Q_e] + \Theta \nabla^2[Q_e]. \quad (\text{S33})$$

Finally, it is crucial to note that Equations (S30) and (S33) are PDEs describing the spatio-temporal dynamics of the concentrations of A and Q in the extra-cellular environment. Parameters for the internal and external signalling molecule dynamics were taken from⁵, and are summarised in Table S7. For the solution of the spatial dynamics (PDEs in Equations (S30) and (S33)), a distance of $20\mu\text{m}$ was chosen between the points corresponding to comparator and target cells.

Parameter	Value	Description
ν_A, ν_Q	0.05 min^{-1}	Synthesis rate of A and Q
η	2 min^{-1}	Cell wall diffusion rate of A and Q
$\gamma_{A,i}, \gamma_{Q,i}$	0.4 min^{-1}	Internal degradation of A and Q
$\gamma_{A,e}, \gamma_{Q,e}$	0.2 min^{-1}	External A and Q degradation
Θ	$4.9e - 10 \text{ m}^2 \text{ sec}^{-1}$	external diffusion rate of A and Q

Supplementary Table S7: Parameter values for signalling molecules.

References

1. Uri Alon. *An introduction to systems biology*. Chapman & Hall/CRC, 2007.
2. Frederick K Balagaddé, Hao Song, Jun Ozaki, Cynthia H Collins, Matthew Barnett, Frances H Arnold, Stephen R Quake, and Lingchong You. A synthetic *Escherichia coli* predator-prey ecosystem. *Molecular systems biology*, 4:187, jan 2008. doi: 10.1038/msb.2008.24.
3. Ye Chen, Jae Kyoung Kim, Andrew J Hirning, Krešimir Josić, and Matthew R Bennett. Emergent genetic oscillations in a synthetic microbial consortium. *Science*, 349(6251):986–989, 2015.
4. M B Elowitz and S Leibler. A synthetic oscillatory network of transcriptional regulators. *Nature*, 403(6767):335–8, January 2000. doi: 10.1038/35002125.
5. Gianfranco Fiore, Antoni Matyjaszkiewicz, Fabio Annunziata, Claire Grierson, Nigel J. Savery, Lucia Marucci, and Mario di Bernardo. In-silico analysis and implementation of a multicellular feedback control strategy in a synthetic bacterial consortium. *ACS Synth. Biol.*, 6(3):507–517, 2017. doi: 10.1021/acssynbio.6b00220. PMID: 27997140.
6. Jordi Garcia-Ojalvo, Michael B Elowitz, and Steven H Strogatz. Modeling a synthetic multicellular clock: repressilators coupled by quorum sensing. *Proceedings of the National Academy of Sciences of the United States of America*, 101(30):10955–60, jul 2004. doi: 10.1073/pnas.0307095101.
7. Jason R Kelly, Adam J Rubin, Joseph H Davis, Caroline M Ajo-Franklin, John Cumbers, Michael J Czar, Kim de Mora, Aaron L Gliberman, Dileep D Monie, and Drew Endy. Measuring the activity of BioBrick promoters using an in vivo reference standard. *Journal of biological engineering*, 3:4, January 2009. doi: 10.1186/1754-1611-3-4.
8. Lucia Marucci, Stefania Santini, Mario di Bernardo, and Diego di Bernardo. Derivation, identification and validation of a computational model of a novel synthetic regulatory network in yeast. *Journal of mathematical biology*, 62(5):685–706, May 2011. doi: 10.1007/s00285-010-0350-z.
9. Marco Mauri and Stefan Klumpp. A model for sigma factor competition in bacterial cells. *PLoS computational biology*, 10(10):e1003845, October 2014. doi: 10.1371/journal.pcbi.1003845.
10. Oliver Purcell, N.J. Savery, C.S. Grierson, and Mario di Bernardo. A comparative analysis of synthetic genetic oscillators. *Journal of The Royal Society Interface*, 7(52):1503, June 2010. doi: 10.1098/rsif.2010.0183.

11. Virgil A Rhodius, Thomas H Segall-Shapiro, Brian D Sharon, Amar Ghodasara, Ekaterina Orlova, Hannah Tabakh, David H Burkhardt, Kevin Clancy, Todd C Peterson, Carol A Gross, and Christopher A Voigt. Design of orthogonal genetic switches based on a crosstalk map of σ s, anti- σ s, and promoters. *Molecular systems biology*, 9:702, January 2013. doi: 10.1038/msb.2013.58.
12. Jesse Stricker, Scott Cookson, Matthew R Bennett, William H Mather, Lev S Tsimring, and Jeff Hasty. A fast, robust and tunable synthetic gene oscillator. *Nature*, 456(7221):516–9, nov 2008. doi: 10.1038/nature07389.
13. Baojun Wang, Richard I Kitney, Nicolas Joly, and Martin Buck. Engineering modular and orthogonal genetic logic gates for robust digital-like synthetic biology. *Nature communications*, 2:508, January 2011. doi: 10.1038/ncomms1516.